
GViT: Representing Images as Gaussians for Visual Recognition

Jefferson Hernandez¹, Ruozhen He¹, Guha Balakrishnan¹,
Alexander C. Berg², Vicente Ordonez¹
Rice University¹ University of California, Irvine²

Abstract

We introduce GViT, a classification framework that abandons conventional pixel or patch grid input representations in favor of a compact set of 2D Gaussians. An encoder learns to represent each image with a few hundred Gaussians whose positions, scales, orientations, colors, and opacities are optimized jointly with and used as input to a ViT classifier trained on top of these representations. The gradients of the classifier are reused as constructive guidance, steering the Gaussians toward class-salient regions while a differentiable renderer optimizes an image reconstruction loss. We demonstrate that these 2D Gaussian representations learned with our GViT guidance, using a relatively standard ViT architecture, closely match the performance of a traditional patch-based ViT, reaching a 76.9% top-1 accuracy on Imagenet-1k using a ViT-B architecture.

1 Introduction

In 1957, computer scientist Russell Kirsch and his colleagues at the U.S. National Bureau of Standards made history by scanning the first digital image. This pioneering work introduced the concept of the pixel as the basic unit of visual representation [27] for digital images. Despite significant advancements in computer vision, including the rise of convolutional neural networks [28, 41, 18, 31] and vision transformers (ViTs) [9, 42, 8], the reliance on fixed pixel grids persists. Even though recent self-supervised approaches such as masked autoencoders (MAE) [17] and hierarchical distillation methods (e.g. DINOv2 [37]) have demonstrated impressive image representations, they still operate on low-level pixel (or patch) reconstructions or invariances. This dependence may constrain models from fully capturing the nuanced, continuous structures inherent in natural images [7].

In this work, we introduce GViT, a novel classification framework that replaces traditional pixel or patch-based inputs with a compact set of 2D Gaussians. GViT uses an encoder that learns to represent an image with a collection of 2D Gaussian primitives parameterized by position, scale (covariance), orientation, and color/opacity. We pair this encoder with a standard ViT-based classifier [9] modified to take 2D Gaussians as input instead of patches, and train them end-to-end in a *collaborative optimization game*: classifier gradients highlighting class-discriminative regions steer the Gaussians toward informative scene details. Thus, the encoder learns a task-adapted representation without requiring explicit supervision on where to place Gaussians. Hence, GViT acts as a form of task-driven image compression, discarding redundant background pixels and concentrating capacity where it matters. As a by-product, the layout of learned Gaussians provides visual intuition about the model’s focus, granting natural, light-weight interpretability. In contrast, naively optimizing 2D Gaussians with stochastic gradient descent either scales poorly to thousands of constraints, or allocates Gaussians inefficiently to capture class-relevant details.

The vision community has long explored *mid-level primitives* as an intermediate representation between pixels and objects. Classic superpixel methods [40, 43, 29, 1, 24] segment an image into perceptually coherent regions, providing a representation closer to human-interpretable parts of an

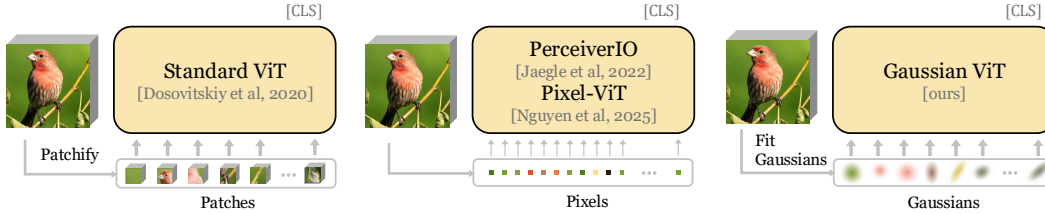


Figure 1: The original Vision Transformer (ViT) [9] model uses a grid of contiguous patch inputs as a representation. Alternative models have explored pixel-level representations [23, 21, 36]. Our work explores the use of Gaussians as our basic primitive. To make training practical in Gaussian space, we train a model that performs Gaussian fitting in a single forward pass as opposed to the iterative optimization method more commonly used in 3D Gaussian Splatting [26].

image. More recently, slot-based models use a set of learned slots to capture object-like entities in a scene without supervision [32, 3, 10], effectively discovering mid-level components. There have been other attempts in *moving beyond pixel-level inputs* in vision models. For example, some works directly model images in the frequency domain to skip superfluous pixel details [38, 16, 49], or feed compressed bytes without full decoding to save computation [19]. Other recent methods tokenize images into discrete visual words (codebook indices) instead of RGB values [2, 51, 35]. These trends reflect a broader push to find input representations that are more semantically structured and computationally efficient than raw pixels. However, our proposal of Gaussian representations has several advantages. Robust implementations of differentiable renderers for Gaussian representations through Gaussian “splatting” are widely available due to the success of this technique in the task of 3D rendering from multiple views [26, 11]. Additionally, Gaussian representations have been recently shown to be effective compressed representations for images [53].

We validate GVIT on standard image classification benchmarks, demonstrating competitive (and sometimes higher) accuracy than pixel-based Vision Transformers while using a significantly reduced input representation. We further analyze the cooperative training dynamics, showing that gradient-guided Gaussians converge to semantically meaningful regions and improve data efficiency. In summary, our contributions are: **(1)** a novel image representation that encodes images as sets of 2D Gaussian primitives, **(2)** a cooperative training scheme in which a ViT classifier guides a differentiable renderer to overcome the scalability and allocation challenges of learning to splat, and **(3)** an empirical demonstration that moving beyond pixels to a task-adapted primitive-based representation yields favorable performance–efficiency trade-offs while naturally offering interpretable visualizations.

Encoding an image as a compact set of Gaussians forces the downstream classifier to strike a new balance between *reconstruction fidelity* and *semantic discrimination*. Inevitably, some fine-grained pixel information is compressed away, and our model trails the strongest patchified ViT baselines by a small margin. A key contribution of this work is the *empirical finding* that alternative mid-level Gaussian-based representations can support competitive recognition, rather than a new architecture. Patch-based ViTs, therefore, should still be the pragmatic choice for large-scale deployment but our results still deliver a clear takeaway that explicit mid-level representations are *viable, interpretable, and surprisingly strong*. We believe that this insight can inform future work devising the next generation of vision backbones, where other intermediate grouped representations can be considered as an alternative between pixel-level and patch-based representations.

2 Method

We propose a mid-level image representation using 2D Gaussians with properties optimized in an end-to-end fashion with a downstream recognition task. Given a large-scale image dataset, we train a small denoising autoencoder [45], to generate Gaussians to be splatted into the images using a differentiable renderer. We perform an iterative *gradient guidance* optimization process, in which a standard ViT classifier [9] and a denoising Gaussian splat network are trained together to produce better representations for downstream tasks. Our method operates directly over the color, center location, scale, and orientation properties of each 2D Gaussian [26]. We render these Gaussians into images with a differentiable renderer, and train the entire model using both a perceptual similarity loss and cross-entropy loss for classification.

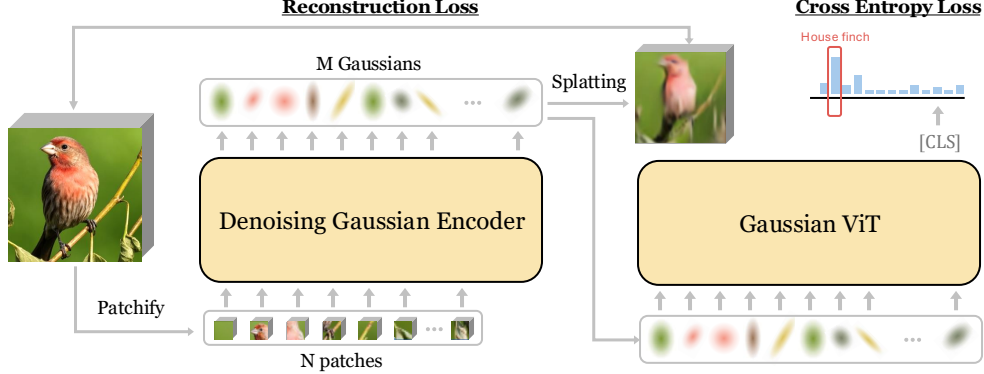


Figure 2: Overview of the training pipeline for GViT. Our model is iteratively trained to recognize patterns in the Gaussian encoded image while a Denoising Gaussian Encoder is trained jointly to reconstruct images using Gaussians. These two models are trained in an alternating fashion.

2.1 Preliminaries

Our method extends the optimization-based single-scene 3D reconstruction of [26] to a 2D setting, representing an image with a set of Gaussians as mid-level representations. Each Gaussian is defined by its center $\mathbf{p} \in \mathbb{R}^2$, covariance $\Sigma \in \mathbb{R}^{2 \times 2}$, color $\mathbf{r} \in \mathbb{R}^3$, and opacity $o \in \mathbb{R}$. Rendering is performed by Gaussian splatting under an orthographic projection with no camera transform, i.e., by treating every Gaussian as lying on its own z -plane and applying standard volumetric splatting. Since the renderer is differentiable, gradients propagate to all Gaussian attributes. We factorize the covariance as $\Sigma = \mathbf{R}\mathbf{S}\mathbf{S}^\top\mathbf{R}^\top$, where $\mathbf{S} = \text{diag}(\mathbf{s})$ with $\mathbf{s} \in \mathbb{R}^2$ and \mathbf{R} is a 2D rotation parameterized by an angle ϕ . Thus one Gaussian is described by the 9-dimensional vector $\mathbf{g} = \mathbf{p}, \mathbf{s}, \phi, \mathbf{r}, o \in \mathbb{R}^9$.

2.2 Denoising Gaussian Encoder

Our pipeline consists of (i) a ViT encoder conditioned on image patches, (ii) a differentiable Gaussian renderer, and (iii) a downstream task head (Fig. 2). An image is split into N patches, embedded, and concatenated with k randomly sampled ‘‘Gaussian tokens’’ $\mathbf{g}_0 \in \mathbb{R}^{k \times 9}$. The encoder maps the resulting sequence to latent vectors $\mathbf{x}_i \in \mathbb{R}^{d_{\text{enc}}}$ for $i = 1, \dots, N + k$. We discard the N image latents and feed the k Gaussian latents to an MLP that predicts a residual

$$\Delta \mathbf{g} = \text{MLP}(\mathbf{x}_{N+1:N+k}), \quad \hat{\mathbf{g}} = \mathbf{g}_0 + \Delta \mathbf{g},$$

mirroring the residual-denoising perspective of diffusion models. We splat the predicted Gaussians $\hat{\mathbf{g}}$ under a fixed orthographic camera to render an image. Following [39], we bound the scale parameters by $\sigma = c \times \text{sigmoid}(\mathbf{s})$, with a constant c . We apply a binary cross-entropy loss between the rendered output and the ground-truth image. Note that using this representation allows us to quickly initialize the Gaussian using unsupervised segmentation methods like KMeans over the colors, and SGD-based segmentation[25] or the Felzenszwalb algorithm [12]. This mirrors typical usages of Gaussian splatting for 3D reconstruction that rely on point-cloud initialization.

Adversarial objectives move pixels along $\nabla_x \mathcal{H}(f(x; \phi), y)$ to *reduce* the true-class logit and induce misclassification, where \mathcal{H} is the cross entropy loss. We apply the **same** gradient but with the *opposite sign*, steering the Gaussians so that class evidence accumulates where it matters.

Notation. $\theta = \{\hat{\mathbf{g}}_j\}_{j=1}^k$ are the Gaussian parameters, $f(\cdot; \phi)$ is the classifier, and y is the ground-truth label. The pixel and perceptual losses are $\mathcal{L}_{\text{pix}}, \mathcal{L}_{\text{perc}}$. For our pixel reconstruction loss L_{pix} , we experiment with MSE (L_{mse}) and binary cross entropy (L_{bce}) and the D-SSIM loss (L_{dssim}) [47] as the perceptual loss $\mathcal{L}_{\text{perc}}$. The classification loss is $L_{\text{cls}} = \mathcal{H}(f(\theta; \phi), y)$.

Relocation gradient (constructive FGSM). We freeze ϕ during the backward pass, obtaining only $\nabla_{\theta} \mathcal{L}_{\text{cls}}$. Adding the *negative* of this gradient to the usual update yields

$$\tilde{\nabla}_{\theta} = \nabla_{\theta} (\mathcal{L}_{\text{pix}} + \lambda_{\text{perc}} \mathcal{L}_{\text{perc}}) - \gamma \nabla_{\theta} \mathcal{L}_{\text{cls}}, \quad (1)$$

where $\gamma \in [0, 0.1]$ controls the strength of the *constructive adversarial* push.

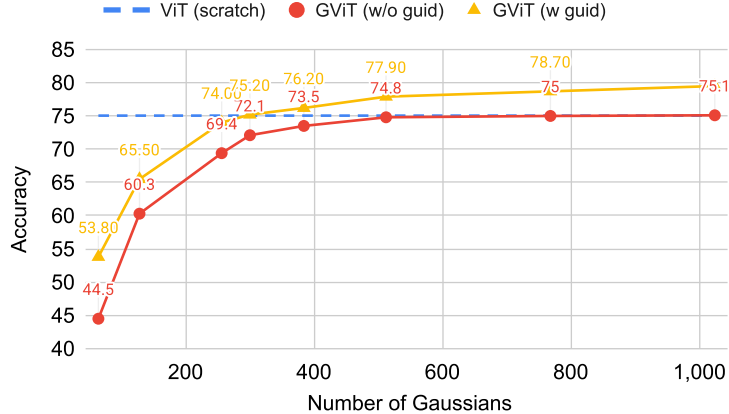


Figure 3: **Number of Gaussians:** Mini-Imagenet classification performance with 64, 128, 256, 512, 768, and 1024 Gaussians per image. As we increase the number of Gaussians, the performance increases monotonically.

Table 1: **Design choices:** Comparing different hyperparameter choices for our method using top-1 accuracy (%) on Mini-Imagenet-100.

Value	top-1	Value	top-1	Loss	top-1	Method	top-1
$c = 0.5$	73.4	$\gamma = 0.025$	72.3	L_{mse}	65.7	Offline	70.5
$c = 0.75$	74.6	$\gamma = 0.05$	73.6	L_{bce}	71.7	Learned queries	71.4
$c = 1.0$	75.2	$\gamma = 0.075$	74.2	$L_{\text{mse}} + L_{\text{dssim}}$	69.8	Denosing	74.8
$c = 2.0$	73.7	$\gamma = 0.1$	75.2	$L_{\text{bce}} + L_{\text{dssim}}$	72.3	Guidance	75.2

(a) Scale factor

(b) Guidance

(c) Reconstruction Loss

(d) Gaussian Fitting

Three-phase training schedule. Our training proceeds as follows:

- (i) **Warm-up:** Update θ using $\mathcal{L}_{\text{pix}} + \mathcal{L}_{\text{perc}}$ only;
- (ii) **Classifier pre-training:** Freeze θ , train C with \mathcal{L}_{cls} so its gradients are informative;
- (iii) **Joint optimization:** Unfreeze all parameters and apply the composite update (1).

By reversing the adversarial-attack direction, we enforce that every gradient step *pulls* Gaussians toward class-salient regions, while the pixel and geometric losses keep the reconstruction faithful.

3 Experiments

We demonstrate the performance of our method on ImageNet-1k and other visual recognition datasets. Our ablations are performed on the mini-ImageNet split from Vinyals *et al.* [46]. All models are trained for 400 epochs. We use a base learning rate of 1×10^{-4} with a cosine scheduler and AdamW [34]. We use PyTorch and train all models in bfloat16 mixed precision. Full ImageNet training takes about 12 hours on 8 NVIDIA Tesla A100 GPUs, each with 48 GB of memory, using DDP [30] to distribute training across GPUs. More details are in the supplemental material.

Architecture. We take the standard ViT [9] conditioned on image patches and experiment with two settings to create the Gaussians: (1) k learnable queries, one for each predicted Gaussian (we discard the predictions made for the image patches), and (2) a denoising model that takes randomly initialized Gaussians and produces residuals to be added to get the final Gaussians. This model has 22M parameters, similar to a ViT/S in size. On top of the learned Gaussians, a ViT classifier is used to obtain the final classification. Since this ViT sees only the Gaussians, it uses fewer computational resources, even though the sequence length might be longer, as Gaussians are represented using 9 parameters. We experiment with the ViT-S/16 and ViT-B/16 configurations.

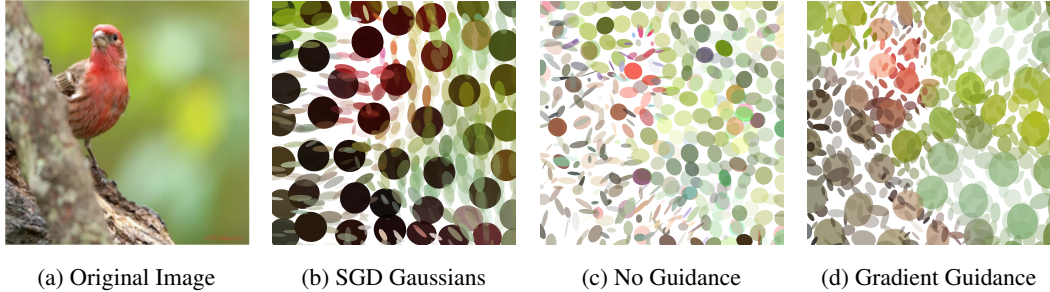


Figure 4: Visualization of Gaussians for a sample image under three training regimes: (a) The original input, (b) Gaussians fitted via reconstruction-only SGD, (c) End-to-end predicted Gaussians without any classifier guidance, and (d) Gaussians steered by classifier-gradient guidance. In this visualization, we show an ellipse sized to 2 standard deviations for each Gaussian.

3.1 Design Considerations

Learning from offline Gaussians. A naïve way to obtain Gaussians is to run a reconstruction-only optimiser such as SGD on every training image, save the converged parameters, and then train the classifier on this frozen set (Fig. 4b). Because the optimiser is blind to semantics, it distributes the positions of Gaussians almost uniformly, forming a quasi-grid without regard to foreground and background. The computation for per-image optimisation and the storage of parameters scale linearly with the dataset—an untenable cost for large-scale datasets like ImageNet-1k. Letting the network predict Gaussians end-to-end (Fig. 4c) removes the preprocessing bottleneck and nudges Gaussians toward higher-level structures, yet the arrangement remains grid-like because supervision is still reconstruction-centric. Our gradient-guidance strategy (Sec. 3.1) closes this gap: classifier gradients actively drag Gaussians into class-salient regions, concentrating capacity where evidence matters and allocating fewer primitives to irrelevant areas (Fig. 4d), all while scaling effortlessly to modern datasets.

The qualitative trends above translate directly into recognition accuracy on Mini-IN-100 (Table 1d). Training on *offline* Gaussians yields a modest 70.5% top-1. Replacing the frozen grid with *learned queries*—but still supervising them only through reconstruction—adds just 0.9 points, confirming that end-to-end prediction alone is not enough. Introducing the *denoising* objective, which perturbs the latent Gaussians and forces the decoder to infer structure, boosts performance to 74.8% by encouraging more informative, non-uniform placements. Finally, our full *gradient guidance* delivers 75.2%, showing that even after strong generative regularisation, explicitly steering Gaussians with classifier gradients provides the last mile of task-specific refinement.

Number of Gaussians. We train six variants that decode 64, 128, 256, 512, 768, and 1,024 Gaussians each and plot Mini-IN-100 top-1 accuracy in Fig. 3. Without gradient guidance (red curve) accuracy climbs from 44.5% at 64 Gaussians to 75.1% at 1,024, but the improvements flatten once the grid exceeds roughly 512 Gaussians. Adding guidance (yellow curve) shifts the entire trade-off upward: the model already surpasses the ViT (trained from scratch) baseline with only 256 Gaussians and continues to improve up to 78.7% at 768, after which performance saturates. These results confirm that gradient-based placement transforms extra Gaussians into meaningful recognition primitives instead of the uniform redundancy one would get from offline Gaussians. We note that we were unable to scale ImageNet training to more than 512 Gaussians and resolutions bigger than 224 by 224 pixels, given the expensive rendering operation. In this sense, our work is to scientifically verify the effectiveness and potential of Gaussians as mid-level representation at an affordable scale, and leave the engineering effort of scaling to higher resolutions or more Gaussians for future work.

Gaussian Scale. The model outputs raw scale parameters that we squash with a sigmoid and multiply by a constant factor c , i.e. $\hat{s} = c \cdot \text{sigmoid}(s)$. This cap prevents randomly-initialized Gaussians from exploding, while still allowing them to grow during training. Table 1a reports Mini-IN-100 accuracy for $c \in \{0.50, 0.75, 1.00, 2.00\}$. Setting $c=0.50$ restricts each Gaussian’s footprint to a few pixels, impeding both reconstruction and recognition (73.4%). Gradually enlarging the bound improves performance and peaks at $c=1.00$ (75.2%), indicating that moderate overlap lets Gaussians cover object parts without washing out detail. Pushing the limit further to $c=2.00$ hurts

Table 2: Top-1 classification accuracies (%) on ImageNet-1K and seven smaller datasets for ViT-S and ViT-B for our Gaussian ViT variants with and without classifier-gradient guidance. For context, we also report ViT models trained on patches with patch sizes 16 and 32 as reported in Steiner *et al.* [42].

Model	IN-1K	Fine-grained Benchmarks							
		AVG	CIFAR-10	CIFAR-100	CUB	SUN397	Flowers	Pets	DTD
<i>Patches with size 32: 7×7 patches</i>									
ViT-S/32	69.2	84.6	-	86.4	92.7	72.9	93.6	91.2	70.7
ViT-B/32	71.4	85.6	-	87.6	92.6	73.8	94.4	92.2	72.7
<i>Patches with size 16: 14×14 patches</i>									
ViT-S/16	77.5	87.8	97.9	86.9	93.1	74.3	95.7	93.8	72.8
ViT-B/16	78.7	85.7	98.1	87.8	93.0	75.3	97.6	93.2	77.8
<i>Gaussians – No guidance</i>									
GViT-S	68.3	75.8	92.3	79.4	86.3	63.9	89.3	86.4	71.4
GViT-B	73.6	81.0	96.6	85.7	88.3	67.1	92.3	92.2	71.9
<i>Gaussians – Classifier guidance</i>									
GViT-S	72.4	78.5	95.3	80.2	88.5	65.9	94.8	89.0	72.9
GViT-B	76.9	83.6	98.6	87.7	91.2	68.3	96.0	94.5	73.4

optimization, as large Gaussians blur fine structure, dropping accuracy to 73.7%. Hence, a unit scale factor offers the best trade-off between expressive coverage and stable learning.

Guidance coefficient During the collaborative learning phase classifier gradients are added to the generator update with weight γ , effectively controlling how far each Gaussian is nudged at every step. Table 1b sweeps $\gamma_{\text{guid}} \in \{0.025, 0.05, 0.075, 0.10\}$. When the coefficient is too small ($\gamma_{\text{guid}} = 0.025$) the Gaussians hardly move, leaving the model close to its unguided baseline and yielding only 71.2% top-1. Increasing the weight allows Gaussians to realign with class-salient regions and steadily improves accuracy—72.6% at 0.05 and 73.3% at 0.075. The best result, 74.8%, is reached with $\gamma_{\text{guid}} = 0.10$, after which we observe overshooting and occasional NaNs during training. Hence, a moderate guidance strength strikes the ideal balance between inertia and instability.

Loss function Gaussian-splat pipelines traditionally rely on a pixel-wise mean-squared error (MSE) between the rendered canvas and the target image, yet this objective is agnostic to class semantics and often encourages overly smooth reconstructions. We test four loss variants: (i) pixel-wise mean-squared error (L_{mse}); (ii) $L_{\text{mse}} + L_{\text{dssim}}$; (iii) pixel-wise binary cross-entropy (L_{bce}); and (iv) $L_{\text{bce}} + L_{\text{dssim}}$. Table 1c summarises the effect on Mini-IN-100 top-1. Pure MSE performs worst at 65.7%, while switching to BCE alone lifts accuracy to 71.7%. Adding DSSIM sharpens the reconstructions and narrows the gap: MSE+DSSIM climbs to 69.8%, and CE+DSSIM attains the best 72.3%. In practice, we adopt the CE+DSSIM combination, which preserves structural detail without sacrificing classification performance.

3.2 Leakage avoidance

To probe whether the *Gaussian encoder* embeds any “hidden” cues that the classifier might exploit beyond the intended geometry–appearance statistics, we designed two complementary tests.

Experiment 1 – Cross-training sanity-check. We first generated two frozen collections of Gaussians: (i) *SGD* Gaussians obtained by running an image–reconstruction optimiser on each training image, and (ii) *learned* Gaussians produced by our gradient-guided encoder. A lightweight ViT-S classifier trained on the SGD Gaussians reached **70.5%** Mini-IN-100 top-1 accuracy on its native representation and **67.4%** when evaluated on the learned Gaussians. Conversely, the classifier trained on the learned representation achieved **71.4%** on its own Gaussians and **68.5%** on the SGD ones.

Table 3: Comparison of Top-1 accuracies (%) on ImageNet-1K against other non-patch input representations including: JPEG bytes, Discrete Cosine Transform (DCT) Coefficients, and Raw Pixels. While some of these models employ different architectures to adapt to the type of input, Pixel-ViT-B/1 [36] provides a model with the most similar architecture based on ViT-B.

Model	Input	IN-1K
ByteFormer-Ti ^{JPEG} [19] <i>TMLR'24</i>	JPEG bytes	64.9
bGPT ^{IN-1K} [48] <i>arXiv'24</i>	JPEG bytes	66.5
JPEG-Ti [38] <i>CVPR'23</i>	DCT coeff.	75.1
JPEG-S [38] <i>CVPR'23</i>	DCT coeff.	76.5
Perceiver [23] <i>ICML'21</i>	Raw pixels	67.6
Perceiver-IO [22] <i>ICLR'22</i>	Raw pixels	72.7
Pixel-ViT-B/1 [36] <i>ICLR'25</i>	Raw pixels	76.1
GViT-B (ours)	Gaussians	76.9

Table 4: Accuracy when the classifier is trained on Gaussians (GS) versus rasterised renderings of those Gaussians (IMG). Consistent gaps ($\approx 2-3$ points) confirm that direct access to the parametric Gaussians helps, yet comparable rankings across settings argue against hidden information leakage.

Setup	mini-IN-100 (GS)	mini-IN-100 (IMG)
Trained on SGD Gaussians	70.5	68.5
Trained on Learned Gaussians	67.6	65.0
Trained under Denoising	71.4	70.5
Training with Guidance	72.1	71.0

This can be understood as a 2×2 confusion matrix. The strong diagonal and similar ≈ 3 -point drop in the off-diagonals indicate that the classifier relies primarily on class-relevant structure present in either Gaussian set rather than memorizing particular “cheat code” artifacts in a particular encoding.

Experiment 2 – Rasterization control. If the Gaussian parameters carried imperceptible cues, *rendering* them to pixels (which discards those parameters) should significantly hurt accuracy. Table 4 shows that scores fall by a modest 2–3 points, but the relative ranking of approaches is preserved, suggesting that a decisive “cheat-code” is not being used. This coherence reinforces our hypothesis that the classifier learns from the genuine content encoded by the Gaussians.

4 Analysis

Main result.

Table 2 shows that *classifier-guided Gaussian relocation lets GViT achieve nearly all of the accuracy that is usually lost when moving away from raw pixels, while keeping the model compact and geometrically interpretable.*

With the same 86 M-parameter backbone, **GViT-B + guidance** attains **76.9 %** top-1 on IN-1k—only 1.8 points below the pixel-based ViT-B/16 (78.7 %). Switching guidance off drops accuracy to 73.6 %, underlining that guidance gradients are doing the heavy lifting. The 22 M variant follows the same pattern: 72.4 % (w/ guidance) vs. 68.3 % (w/o). Both guided models outperform alternative mid-level approaches such as JPEG-S (76.5 %) or Perceiver-IO (72.7 %).

We freeze the Gaussian *generator* learned on ImageNet and fine-tune only the classifier head on ten specialist benchmarks. Guidance once more pays dividends: averaged across tasks, GViT-B climbs from 81.0 % to **83.6 %**, rivalling the IN-1k-pretrained ViT-S/16 despite processing $\sim 4\times$ fewer input tokens. Gains are most pronounced on datasets where objects occupy a small fraction of the frame (e.g. +3.2 points on Aircraft, +1.2 points on Cars), validating our hypothesis that gradient-driven Gaussians concentrate capacity where it matters.

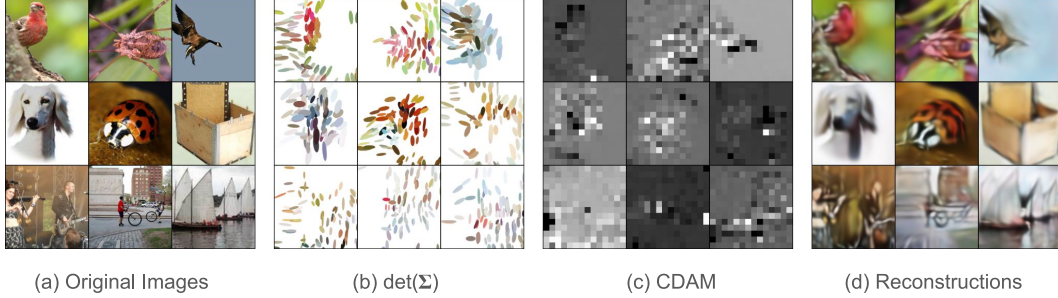


Figure 5: Gradient-guided Gaussians exhibit a natural interpretability component. (a) Original input images. (b) Determinant of the covariance ($\det(\Sigma)$), which clusters Gaussian primitives in class-salient regions. (c) Class-Discriminative Attention Maps (CDAM) over the learned Gaussians. (d) Reconstructions obtained from the Gaussian representation.

The *same* Gaussian encoder trained jointly with a ViT-S classifier easily transfers to ViT-B: we simply replace the classifier, resume training, and lower the guidance weight to $\gamma = 0.05$ (from 0.10) for stability. This shortcut halves the end-to-end training time for GViT-B with no measurable loss to accuracy. Likewise, because Gaussians are dataset-agnostic, adapting to a new benchmark only requires fine-tuning the classifier with roughly 5% of the FLOPs needed to retrain a full pixel-ViT.

Explainability of the Gaussians. An advantage of representing an image with 2D Gaussians is that every primitive carries an explicit geometric scale through its covariance Σ . During training, we observed a consistent *shrinking-for-saliency* effect: gradients that maximize the class log-likelihood also minimize the volume of Gaussians that support the decision. Empirically, the determinant $\det(\Sigma)$ is therefore a proxy for importance, where Gaussians with smaller values cluster around class-discriminative regions, and those with larger values tend to spread over background (Fig. 5 (b)).

To corroborate this geometric signal, we use *Class-Discriminative Attention Maps* (CDAM) following Brocki *et al.* [4]. For target class c , the contribution of the i -th Gaussian token g_i is defined as $S_{i,c} = \sum_j g_{ij} \frac{\partial f_c}{\partial g_{ij}}$, where g_{ij} denotes the j -th element of the Gaussians fed to the last attention layer. We project these scores onto a 16×16 grid by assigning $S_{i,c}$ to the cell that contains a Gaussian center; empty cells receive 0. The resulting heatmaps (Fig. 5 (c)) tightly overlap the low- $\det(\Sigma)$ clusters while revealing finer part-level structure (e.g. the bird’s head, the violin neck), showing that both cues identify the same high-evidence regions from complementary perspectives.

Why does guidance help? We now linearize the classifier *directly* in the Gaussian parameter space. Let $\theta \in \mathbb{R}^d$ denote the flattened vector of all learnable Gaussian parameters, let $\mathbf{w} \in \mathbb{R}^d$ denote the classifier weight vector acting on those parameters, and let σ denote softmax. Then:

$$s(\theta) = \mathbf{w}^\top \theta, \quad \mathcal{L}_{\text{cls}}(\theta, y) = \mathcal{H}(\sigma(s(\theta)), y).$$

Constructive FGSM in parameter space. Constrain updates to an ℓ_∞ budget of $\|\Delta\theta\|_\infty \leq \varepsilon$ for some $\varepsilon > 0$. The logit increase is maximised by

$$\Delta\theta^* = \max_{\Delta\theta} \nabla_\theta \mathcal{H}(\theta; w)^\top \Delta\theta + \mathcal{H}(\theta; w) \quad \text{s.t.} \quad \|\Delta\theta\|_\infty \leq \varepsilon = \varepsilon \text{sign}(\mathbf{w})$$

This implies $s(\theta + \Delta\theta^*) - s(\theta) = \varepsilon \|\mathbf{w}\|_1$. and because $\|\mathbf{w}\|_1$ grows *linearly* with $d = 9k$, even an infinitesimal parameter nudge yields a macroscopic rise of the true-class logit – the same dimensionality argument that explains adversarial examples [14], but now used *to help*, not hurt, classification.

Competition between reconstruction and recognition. Let $\mathcal{L}_{\text{rec}}(\theta) = \mathcal{L}_{\text{pix}} + \lambda_{\text{perc}} \mathcal{L}_{\text{perc}}$ be the reconstruction loss. Its gradient $\nabla_\theta \mathcal{L}_{\text{rec}}$ can be nearly orthogonal (or even opposed) to \mathbf{w} —Gaussians may freeze on background details that reconstruct well but are weakly informative for the class. We therefore apply a *constructive adversarial* update

$$\tilde{\nabla}_\theta = \nabla_\theta \mathcal{L}_{\text{rec}} - \gamma \mathbf{w}, \quad (2)$$

where $\gamma \in [0, 0.1]$ modulates guidance strength. Setting $\gamma > 0$ ensures a descent step for cross-entropy,

$$\mathcal{L}_{\text{cls}}(\theta - \eta \tilde{\nabla}_\theta) < \mathcal{L}_{\text{cls}}(\theta) \quad \text{for small step } \eta > 0,$$

while perturbing \mathcal{L}_{rec} only mildly, thanks to the Lipschitz continuity of both losses. Because the Gaussian parameter space is high-dimensional and the renderer exposes a smooth Jacobian, infinitesimal moves along $-\nabla_{\theta}\mathcal{L}_{\text{cls}}$ translate into significant gains in the true-class logit. Equation (2) therefore acts as a *constructive adversarial regularizer*, preserving fidelity (via \mathcal{L}_{rec}) while systematically steering the representation toward features that the linearized classifier values most.

5 Related Work

Structured image representations: Beyond latent-code decoders, a growing body of work argues that *explicit, differentiable* primitives provide a more interpretable and manipulable canvas for visual understanding. Superpixel Sampling Networks (SSN) [24] substitute raw pixels with learnable superpixels, greatly reducing the number of primitives while staying end-to-end trainable. Slot Attention [32] introduces a permutation-invariant set of *slots* that dynamically bind to individual objects and enable compositional scene understanding. Pushing this idea to finer granularity, Leopart [54] clusters Vision-Transformer tokens in a dense, self-supervised manner to discover object *parts*. Geometry-aware view-synthesis methods such as Multi-Plane Images (MPI) [44] encode a scene as a stack of front-parallel RGBA planes and can be learned from single photographs. The recently proposed Gaussian MAE [39] predicts a cloud of 3D Gaussians from masked input as a pretext task for pixel reconstruction and discards them at inference. In contrast, GVIT uses 2D Gaussians as inputs during inference and actively steers them toward class-salient regions via classifier-gradient guidance.

Beyond pixels Vision: Several recent approaches learn directly from *non-pixel* data. Park *et al.* introduce *RGB No More* Vision Transformers, which ingest minimally decoded JPEG DCT coefficients and therefore slash I/O and compute overhead without sacrificing accuracy [38]. Horton *et al.* generalize this idea with BYTEFORMER, showing that a single Transformer operating on raw file *bytes* can classify images, audio, and other modalities competitively, dispensing with any modality-specific pre-processing [19]. Most recently, Wu *et al.* demonstrate that next-byte prediction scales to universal “digital-world simulators”: their bGPT model matches specialized systems across various binary formats while remaining purely byte-level [48]. Although these methods break free from pixel grids, their resulting latent byte representations are opaque. By contrast, we encode each scene with a compact set of 2D Gaussians whose spatial extents, colors, and opacities are *human-interpretable*, yet deliver improved recognition performance compared to using raw bytes as inputs.

6 Conclusion and Limitations

We introduce GVIT, a vision-transformer framework that learns to represent images with a compact set of 2D Gaussians while learning to classify images from this representation. Guided by gradients of the classifier, these primitives migrate toward class-salient regions, yielding an interpretable mid-level representation that preserves task performance while compressing the representation. Across ImageNet-1k and eight fine-grained transfer datasets, GVIT matches or exceeds similarly sized patchified ViTs and exposes geometric structure that can be inspected, masked, or edited. Despite these encouraging results, the approach is subject to several limitations. The total number of Gaussians is fixed before training. Choosing this budget incorrectly either starves the model of capacity or inflates memory and compute. Second, Gaussians are static after the gradient-guidance phase, preventing the network from dynamically spawning or reallocating them.

Rendering the Gaussians to an image using the differentiable renderer introduces an additional $O(kHW)$ cost and non-negligible GPU memory overhead, which currently limits training scalability for high resolutions or dense prediction tasks. Finally, performance is sensitive to hyperparameters, including the guidance coefficient, covariance max size, and training schedule. However we believe that our work offers a new path to formulate novel model explainability and model architecture designs that are specifically tailored for Gaussian representations.

While Gaussian-based representations may not yet deliver improved performance over standard patch-based inputs, our work signals that patches are a convenient design choice, but *not* a fundamental requirement. Moreover, using individual pixels as tokens while shown to work, incurs a significantly larger overhead over context length and our proposed Gaussian representations offer an alternative mid-level representation between pixel-level and patch-level inputs.

References

- [1] Radhakrishna Achanta, Appu Shaji, Kevin Smith, Aurélien Lucchi, Pascal Fua, and Sabine Süsstrunk. Slic superpixels compared to state-of-the-art superpixel methods. *IEEE Transactions on Pattern Analysis and Machine Intelligence*, 34(11):2274–2282, 2012.
- [2] Hangbo Bao, Li Dong, Songhao Piao, and Furu Wei. Beit: Bert pre-training of image transformers. *arXiv preprint arXiv:2106.08254*, 2021.
- [3] Ondrej Biza, Sjoerd Van Steenkiste, Mehdi S. M. Sajjadi, Gamaleldin Fathy Elsayed, Aravindh Mahendran, and Thomas Kipf. Invariant slot attention: Object discovery with slot-centric reference frames. In Andreas Krause, Emma Brunskill, Kyunghyun Cho, Barbara Engelhardt, Sivan Sabato, and Jonathan Scarlett, editors, *Proceedings of the 40th International Conference on Machine Learning*, volume 202 of *Proceedings of Machine Learning Research*, pages 2507–2527. PMLR, 23–29 Jul 2023.
- [4] Lennart Brocki, Jakub Binda, and Neo Christopher Chung. Class-discriminative attention maps for vision transformers. *arXiv preprint arXiv:2312.02364*, 2023.
- [5] Mark Chen, Alec Radford, Rewon Child, Jeffrey Wu, Heewoo Jun, David Luan, and Ilya Sutskever. Generative pretraining from pixels. In *International conference on machine learning*, pages 1691–1703. PMLR, 2020.
- [6] Kevin Clark, Minh-Thang Luong, Quoc V Le, and Christopher D Manning. Electra: Pre-training text encoders as discriminators rather than generators. *arXiv preprint arXiv:2003.10555*, 2020.
- [7] Timothée Darcet, Maxime Oquab, Julien Mairal, and Piotr Bojanowski. Vision transformers need registers. In *The Twelfth International Conference on Learning Representations*, 2024.
- [8] Mostafa Dehghani, Josip Djolonga, Basil Mustafa, Piotr Padlewski, Jonathan Heek, Justin Gilmer, Andreas Peter Steiner, Mathilde Caron, Robert Geirhos, Ibrahim Alabdulmohsin, et al. Scaling vision transformers to 22 billion parameters. In *International Conference on Machine Learning*, pages 7480–7512. PMLR, 2023.
- [9] Alexey Dosovitskiy, Lucas Beyer, Alexander Kolesnikov, Dirk Weissenborn, Xiaohua Zhai, Thomas Unterthiner, Mostafa Dehghani, Matthias Minderer, G Heigold, S Gelly, et al. An image is worth 16x16 words: Transformers for image recognition at scale. In *International Conference on Learning Representations*, 2020.
- [10] Ke Fan, Zechen Bai, Tianjun Xiao, Tong He, Max Horn, Yanwei Fu, Francesco Locatello, and Zheng Zhang. Adaptive slot attention: Object discovery with dynamic slot number. In *Proceedings of the IEEE/CVF Conference on Computer Vision and Pattern Recognition*, pages 23062–23071, 2024.
- [11] Ben Fei, Jingyi Xu, Rui Zhang, Qingyuan Zhou, Weidong Yang, and Ying He. 3d gaussian splatting as new era: A survey. *IEEE Transactions on Visualization and Computer Graphics*, 2024.
- [12] Pedro F Felzenszwalb and Daniel P Huttenlocher. Efficient graph-based image segmentation. *International journal of computer vision*, 59:167–181, 2004.
- [13] Xavier Glorot and Yoshua Bengio. Understanding the difficulty of training deep feedforward neural networks. In *Proceedings of the thirteenth international conference on artificial intelligence and statistics*, pages 249–256. JMLR Workshop and Conference Proceedings, 2010.
- [14] Ian J Goodfellow, Jonathon Shlens, and Christian Szegedy. Explaining and harnessing adversarial examples. *arXiv preprint arXiv:1412.6572*, 2014.
- [15] Priya Goyal, Piotr Dollár, Ross Girshick, Pieter Noordhuis, Lukasz Wesolowski, Aapo Kyrola, Andrew Tulloch, Yangqing Jia, and Kaiming He. Accurate, large minibatch sgd: Training imagenet in 1 hour. *arXiv preprint arXiv:1706.02677*, 2017.
- [16] Lionel Gueguen, Alex Sergeev, Ben Kadlec, Rosanne Liu, and Jason Yosinski. Faster neural networks straight from jpeg. *Advances in Neural Information Processing Systems*, 31, 2018.

- [17] Kaiming He, Xinlei Chen, Saining Xie, Yanghao Li, Piotr Dollár, and Ross Girshick. Masked autoencoders are scalable vision learners. In *Proceedings of the IEEE/CVF conference on computer vision and pattern recognition*, pages 16000–16009, 2022.
- [18] Kaiming He, Xiangyu Zhang, Shaoqing Ren, and Jian Sun. Deep residual learning for image recognition. In *Proceedings of the IEEE Conference on Computer Vision and Pattern Recognition (CVPR)*, CVPR '16, pages 770–778, June 2016.
- [19] Maxwell Horton, Sachin Mehta, Ali Farhadi, and Mohammad Rastegari. Bytes are all you need: Transformers operating directly on file bytes. *Transactions of Machine Learning Research (TMLR)*, 2024.
- [20] Binbin Huang, Zehao Yu, Anpei Chen, Andreas Geiger, and Shenghua Gao. 2d gaussian splatting for geometrically accurate radiance fields. In *ACM SIGGRAPH 2024 conference papers*, pages 1–11, 2024.
- [21] Andrew Jaegle, Sebastian Borgeaud, Jean-Baptiste Alayrac, Carl Doersch, Catalin Ionescu, David Ding, Skanda Koppula, Daniel Zoran, Andrew Brock, Evan Shelhamer, et al. Perceiver IO: A General Architecture for Structured Inputs & Outputs. In *International Conference on Learning Representations (ICLR)*, 2022.
- [22] Andrew Jaegle, Sebastian Borgeaud, Jean-Baptiste Alayrac, Carl Doersch, Catalin Ionescu, David Ding, Skanda Koppula, Daniel Zoran, Andrew Brock, Evan Shelhamer, Olivier J Henaff, Matthew Botvinick, Andrew Zisserman, Oriol Vinyals, and Joao Carreira. Perceiver IO: A general architecture for structured inputs & outputs. In *International Conference on Learning Representations*, 2022.
- [23] Andrew Jaegle, Felix Gimeno, Andy Brock, Oriol Vinyals, Andrew Zisserman, and Joao Carreira. Perceiver: General Perception with Iterative Attention. In *International conference on machine learning*, pages 4651–4664. PMLR, 2021.
- [24] Varun Jampani, Deqing Sun, Ming-Yu Liu, Ming-Hsuan Yang, and Jan Kautz. Superpixel sampling networks. In *Proceedings of the European Conference on Computer Vision (ECCV)*, pages 352–368, 2018.
- [25] Asako Kanezaki. Unsupervised image segmentation by backpropagation. In *2018 IEEE international conference on acoustics, speech and signal processing (ICASSP)*, pages 1543–1547. IEEE, 2018.
- [26] Bernhard Kerbl, Georgios Kopanas, Thomas Leimkühler, and George Drettakis. 3d gaussian splatting for real-time radiance field rendering. *ACM Transactions on Graphics*, 42(4):1–14, 2023.
- [27] Russell A Kirsch. Seac and the start of image processing at the national bureau of standards. *IEEE Annals of the History of Computing*, 20(2):7–13, 1998.
- [28] Alex Krizhevsky, Ilya Sutskever, and Geoffrey E. Hinton. Imagenet classification with deep convolutional neural networks. In F. Pereira, C. J. C. Burges, L. Bottou, and K. Q. Weinberger, editors, *Advances in Neural Information Processing Systems 25*, pages 1097–1105. Curran Associates, Inc., 2012.
- [29] Alex Levinshtein, Adrian Stere, Kiriakos N. Kutulakos, David J. Fleet, Sven J. Dickinson, and Kaleem Siddiqi. Turbopixels: Fast superpixels using geometric flows. *IEEE Transactions on Pattern Analysis and Machine Intelligence*, 31(12):2290–2302, 2009.
- [30] Shen Li, Yanli Zhao, Rohan Varma, Omkar Salpekar, Pieter Noordhuis, Teng Li, Adam Paszke, Jeff Smith, Brian Vaughan, Pritam Damania, et al. Pytorch distributed: Experiences on accelerating data parallel training. *arXiv preprint arXiv:2006.15704*, 2020.
- [31] Zhuang Liu, Hanzi Mao, Chao-Yuan Wu, Christoph Feichtenhofer, Trevor Darrell, and Saining Xie. A convnet for the 2020s. In *Proceedings of the IEEE/CVF Conference on Computer Vision and Pattern Recognition (CVPR)*, pages 11976–11986, June 2022.

- [32] Francesco Locatello, Dirk Weissenborn, Thomas Unterthiner, Aravindh Mahendran, Georg Heigold, Jakob Uszkoreit, Alexey Dosovitskiy, and Thomas Kipf. Object-centric learning with slot attention. *Advances in neural information processing systems*, 33:11525–11538, 2020.
- [33] Ilya Loshchilov and Frank Hutter. Sgdr: Stochastic gradient descent with warm restarts. In *International Conference on Learning Representations*, 2016.
- [34] Ilya Loshchilov and Frank Hutter. Decoupled weight decay regularization. *arXiv preprint arXiv:1711.05101*, 2017.
- [35] Xiaofeng Mao, Yuefeng Chen, Ranjie Duan, Yao Zhu, Gege Qi, Shaokai Ye, Xiaodan Li, Rong Zhang, and Hui Xue. Enhance the visual representation via discrete adversarial training. *arXiv preprint arXiv:2209.07735*, 2022.
- [36] Duy-Kien Nguyen, Mahmoud Assran, Unnat Jain, Martin R Oswald, Cees GM Snoek, and Xinlei Chen. An image is worth more than 16x16 patches: Exploring transformers on individual pixels. *International Conference on Learning Representations (ICLR)*, 2025.
- [37] Maxime Oquab, Timothée Darcet, Théo Moutakanni, Huy V. Vo, Marc Szafraniec, Vasil Khalidov, Pierre Fernandez, Daniel HAZIZA, Francisco Massa, Alaaeldin El-Nouby, Mido Assran, Nicolas Ballas, Wojciech Galuba, Russell Howes, Po-Yao Huang, Shang-Wen Li, Ishan Misra, Michael Rabbat, Vasu Sharma, Gabriel Synnaeve, Hu Xu, Herve Jegou, Julien Mairal, Patrick Labatut, Armand Joulin, and Piotr Bojanowski. DINOv2: Learning robust visual features without supervision. *Transactions on Machine Learning Research*, 2024. Featured Certification.
- [38] Jeongsoo Park and Justin Johnson. Rgb no more: Minimally-decoded jpeg vision transformers. In *Proceedings of the IEEE/CVF Conference on Computer Vision and Pattern Recognition*, pages 22334–22346, 2023.
- [39] Jathushan Rajasegaran, Xinlei Chen, Rulilong Li, Christoph Feichtenhofer, Jitendra Malik, and Shiry Ginosar. Gaussian masked autoencoders. *arXiv preprint arXiv:2501.03229*, 2025.
- [40] Xiaofeng Ren and Jitendra Malik. Learning a classification model for segmentation. In *Proceedings Ninth IEEE International Conference on Computer Vision (ICCV)*, pages 10–17. IEEE, 2003.
- [41] Karen Simonyan and Andrew Zisserman. Very deep convolutional networks for large-scale image recognition. *CoRR*, abs/1409.1556, 2014.
- [42] Andreas Peter Steiner, Alexander Kolesnikov, Xiaohua Zhai, Ross Wightman, Jakob Uszkoreit, and Lucas Beyer. How to train your vit? data, augmentation, and regularization in vision transformers. *Transactions on Machine Learning Research*, 2022.
- [43] David Stutz, Alexander Hermans, and Bastian Leibe. Superpixels: An evaluation of the state-of-the-art. *Computer Vision and Image Understanding*, 166:1–27, 2018.
- [44] Richard Tucker and Noah Snavely. Single-view view synthesis with multiplane images. In *Proceedings of the IEEE/CVF Conference on Computer Vision and Pattern Recognition*, pages 551–560, 2020.
- [45] Pascal Vincent, Hugo Larochelle, Isabelle Lajoie, Yoshua Bengio, Pierre-Antoine Manzagol, and Léon Bottou. Stacked denoising autoencoders: Learning useful representations in a deep network with a local denoising criterion. *Journal of machine learning research*, 11(12), 2010.
- [46] Oriol Vinyals, Charles Blundell, Timothy Lillicrap, Daan Wierstra, et al. Matching networks for one shot learning. *Advances in neural information processing systems*, 29, 2016.
- [47] Zhou Wang, Alan C Bovik, Hamid R Sheikh, and Eero P Simoncelli. Image quality assessment: from error visibility to structural similarity. *IEEE transactions on image processing*, 13(4):600–612, 2004.
- [48] Shangda Wu, Xu Tan, Zili Wang, Rui Wang, Xiaobing Li, and Maosong Sun. Beyond language models: Byte models are digital world simulators. *arXiv preprint arXiv:2402.19155*, 2024.

- [49] Kai Xu, Minghai Qin, Fei Sun, Yuhao Wang, Yen-Kuang Chen, and Fengbo Ren. Learning in the frequency domain. In *Proceedings of the IEEE/CVF conference on computer vision and pattern recognition*, pages 1740–1749, 2020.
- [50] Vickie Ye, Ruilong Li, Justin Kerr, Matias Turkulainen, Brent Yi, Zhuoyang Pan, Otto Seiskari, Jianbo Ye, Jeffrey Hu, Matthew Tancik, and Angjoo Kanazawa. gsplat: An open-source library for gaussian splatting. *Journal of Machine Learning Research*, 26(34):1–17, 2025.
- [51] Jiahui Yu, Xin Li, Jing Yu Koh, Han Zhang, Ruoming Pang, James Qin, Alexander Ku, Yuanzhong Xu, Jason Baldridge, and Yonghui Wu. Vector-quantized image modeling with improved vqgan. *arXiv preprint arXiv:2110.04627*, 2021.
- [52] Chaoning Zhang, Chenshuang Zhang, Junha Song, John Seon Keun Yi, Kang Zhang, and In So Kweon. A survey on masked autoencoder for self-supervised learning in vision and beyond. *arXiv preprint arXiv:2208.00173*, 2022.
- [53] Xinjie Zhang, Xingtong Ge, Tongda Xu, Dailan He, Yan Wang, Hongwei Qin, Guo Lu, Jing Geng, and Jun Zhang. Gaussianimage: 1000 fps image representation and compression by 2d gaussian splatting. In *European Conference on Computer Vision*, pages 327–345. Springer, 2024.
- [54] Adrian Ziegler and Yuki M Asano. Self-supervised learning of object parts for semantic segmentation. In *Proceedings of the IEEE/CVF conference on computer vision and pattern recognition*, pages 14502–14511, 2022.

A Implementation Details

We will release code and model checkpoints, along with the specific training configurations. We followed previous training configurations that also worked well for ViTs [9, 42]. The pseudocode of GViT is also provided in Algorithm 1.

We follow the standard ViT architecture [9], which has a stack of Transformer blocks, each of which consists of a multi-head attention block and a Multi-Layer Perceptron (MLP) block, with Layer Normalization (LN). A linear projection layer is used after the Gaussian Encoder to match the width of the Gaussian classifier. We use learned position embeddings for both the encoder and classifier. We use the class token from the original ViT architecture, but notice that similar results are obtained without it (using average pooling). We use `gsplat` [50] as our differentiable renderer library, we use their implementation of 2DGS [20], but fix the z -coordinate to the $z = 0$ plane and only allow rotations in the x - y plane by fixing $x = 0$ and $y = 0$ in the quaternion vector.

ImageNet-1k Pre-training. The default settings can be found in Table A.1a. We do not perform any color augmentation, path dropping or gradient clipping. We initialize our transformer layer using `xavier_uniform` [13], as it is standard for Transformer architectures. We use the linear learning rate (lr) scaling rule so that $lr = base_lr \times batchsize / 256$ [15]. Our *guidance* loss schedule is as follows: we train the Gaussian encoder on its own for 150 epochs, we add the perceptual loss \mathcal{L}_{perc} with a weight of 0.1, and train for another 50 epochs, we add the Gaussian classifier and train together with the Gaussians encoder for 100 epochs, we finally add the guidance gradient at the last 50 epochs of training with $\gamma = 0.1$, performing 10 normal training steps for every step of guidance. Our *no-guidance* loss schedule is the same as before but with no guidance added for the last 50 epochs.

Transfer to other datasets. We follow common practice for end-to-end finetuning. Default settings can be found in Table A.1b. Similar to previous work, we use layer-wise lr decay [52].

B More qualitative examples.

We present more qualitative examples of our method on the ImageNet-1k benchmark (See Fig. B.1). These are raw results and not cherry-picked.

Algorithm 1: GViT PyTorch pseudocode.

```

# I[N, C, H, W] - minibatch
# plambda: perceptual coefficient
# clambda: class coefficient
# gamma: guidance coefficient
# scale_factor: scale factor
# kwargs: focal_length, viewmat, Ks, other gsplat args

for step, (I, y) in enumerate(loader):
    # sample random gaussians
    g_ = random_gaussian()
    delta_g = gauss_encoder(I)
    g = g_ + delta_g
    y_hat = gauss_cls(g) # [N, n_gauss, D]
    mu, squats, scale, op, colors = decode_gauss(g)
    I_hat = rasterize(
        mu, squats, scale, op, colors, **kwargs
    )
    # compute pixel loss
    loss_pixel = mse(I_hat, I)
    loss_perc = dssim(I_hat, I)
    loss_cls = ce(y_hat, y)
    # compute final loss
    loss = loss_pixel + plambda * loss_perc + clambda *
        loss_cls
    #normal updates
    opt_enc.zero_grad()
    opt_cls.zero_grad()
    loss.backward()
    opt_enc.step()
    opt_cls.step()
    if step % 10 == 0:
        gauss_cls.requires_grad_(False)
        opt_enc.zero_grad()
        (loss_pix + plambda * loss_perc).backward()
        rec_grads = gauss_encoder.grad
        opt_enc.zero_grad()
        loss_cls.backward()
        cls_grads = gauss_cls.grad
        gauss_encoder.grad = rec_grads + gamma * cls_grads
        opt_enc.step()
        gauss_cls.requires_grad_(True)

def decode_gauss(g):
    mu, squats, scale, op, colors = split(g, [3,4,3,1,3])
    mu = tanh(mu)
    # set z coordinate to 0
    mu[..., -1] = 0
    # only rotate in x,y plane
    quats[..., [1,2]] = 0
    # maximum gauss size
    scales = scale_factor * sigmoid(scales)
    # opacities to 0-1
    op = sigmoid(op)
    # colors to 0-1
    colors = sigmoid(colors)
    return mu, squats, scale, op, colors

```

Table A.1: **Implementation details.** *Left:* ImageNet-1k pre-training settings. *Right:* fine-tuning hyper-parameters for downstream transfer.

(a) ImageNet-1k Pre-training		(b) Transfer to Other Datasets		
config	value	config	ViT/S	ViT/B
optimizer	AdamW [34]	optimizer	AdamW	
base learning rate	1e-4	optimizer momentum	$\beta_1, \beta_2=0.9, 0.999$	
weight decay	0.05	base learning rate		
optimizer momentum	$\beta_{1,2}=0.9, 0.95$ [5]	C10, C100	1e-3	3e-3
batch size	4096	CUB	4.8e-3	
lr schedule	cosine decay [33]	SUN	3.4e-3	4.8e-3
warm-up epochs	10 [15]	Pets, Flowers	1e-3	
epochs	400	DTD	3e-3	
augmentation	hflip, crop [0.5, 1]	weight decay	0.05	
λ_{perc}	0.1	learning rate schedule	cosine decay	
perc-loss schedule	0→0.1 (from epoch 150)	warmup epochs	5	
λ_{cls}	1	layer-wise lr decay [6, 2]	0.65	0.75
		batch size	1024	768
		training epochs		
		C10, C100	60	50
		CUB, SUN	100	80
		Pets, Flowers	100	50
		DTD	50	
		augmentation	hflip, crop [0.5, 1]	

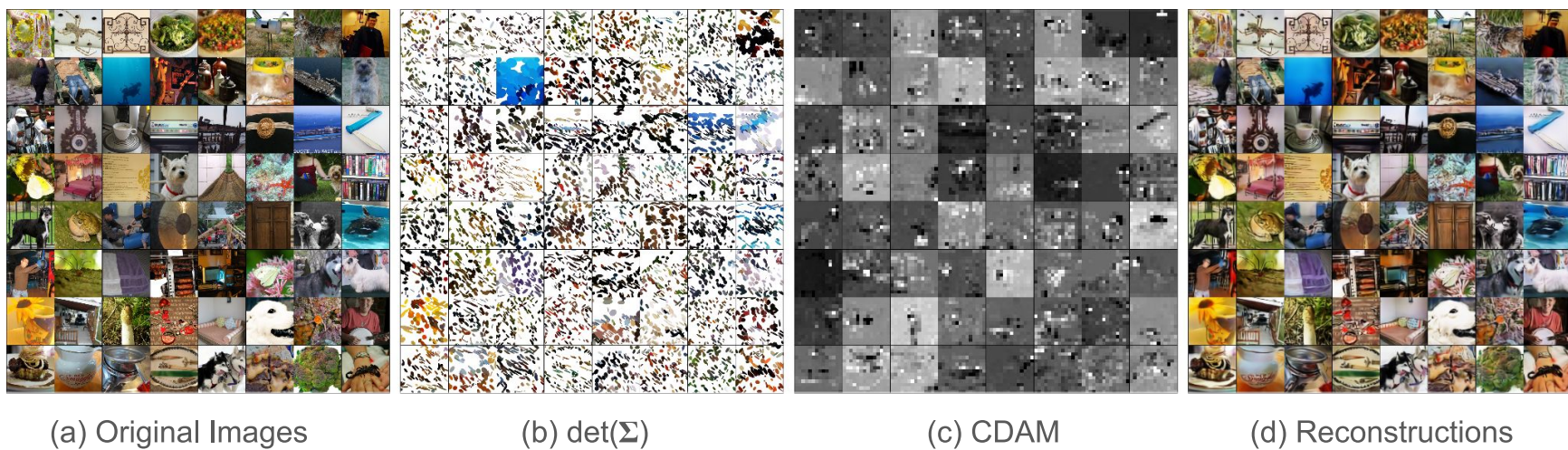


Figure B.1: Gradient-guided Gaussians exhibit a natural interpretability component. (a) Original input images. (b) Determinant of the covariance ($\det(\Sigma)$), which clusters Gaussian primitives in class-salient regions. (c) Class-Discriminative Attention Maps (CDAM) over the learned Gaussians. (d) Reconstructions obtained from the Gaussian representation.